Interfacial disorder-driven metal-insulator transition and enhanced low-temperature magnetoresistance in $La_{0.7}Ca_{0.3}MnO_3/LaNiO_3$ superlattices

Prahallad Padhan and R. C. Budhani
Department of Physics, Indian Institute of Technology Kanpur, Kanpur-208016, India
(Received 9 July 2002; revised manuscript received 10 October 2002; published 17 January 2003)

The temperature- and magnetic-field-dependent resistivity of $La_{0.7}Ca_{0.3}MnO_3/LaNiO_3$ superlattices grown on (001)-oriented $SrTiO_3$ and $LaAlO_3$ substrates is compared as a function of $LaNiO_3$ spacer layer thickness. The electron transport in superlattices with the spacer layer thickness $\leqslant 4$ unit cells is characterized by a thermally activated resistivity $\rho(T)$ between 4.2 and 300 K, and a large ($\sim$90%) magnetoresistance at low temperatures. A parallel resistor model, which explicitly takes into account the interfacial disorder in each unit of the superlattice, correctly reproduces the broad features of the $\rho(T)$ curves. We attribute the disordered interfaces to lattice-mismatch-induced strain and a magnetic roughness, which results from truncation of the three-dimensional coordination of magnetic ions at the interfaces.

DOI: 10.1103/PhysRevB.67.024414 PACS number(s): 75.70.Cn, 75.30.Et, 81.15.Fg, 75.47.Gk

I. INTRODUCTION

Since the discovery of giant magnetoresistance and oscillatory magnetic coupling in superlattices of 3*d* transition metals,[1–3] several attempts have been made to look for similar effects in periodic structures consisting of ferromagnetic and nonmagnetic compounds. Multilayers of magnetic oxides such as the hole-doped manganites, ruthenates, and Fe_3O_4, separated by spacer layers of diverse conductivities and magnetic properties, have been tried.[4–12] However, unlike the case of elemental superlattices, measurements of electron transport and magnetic ordering in these systems have generally yielded mixed results. For example, Gong *et al.*[4] have studied the magnetoresistance (MR) of $La_{0.67}Ca_{0.33}MnO_3$ (LCMO) and $SrRuO_3$ (SRO) superlattices as a function of SRO spacer thickness. Both LCMO and SRO are ferromagnetic metals below their Curie temperatures of $\sim$250 and $\sim$145 K, respectively. No oscillatory behavior of MR is seen as the SRO spacer thickness is increased from one unit cell (UC) to 16 UC. However, the saturation field of these superlattices shows nonmonotonic behavior. Gong *et al.*[4] attributed it to rotation of the magnetic easy axis on the plane of the multilayer. Orozco *et al.*[5] reported oscillatory magnetic coupling in multilayers of the ferromagnetic semiconductor Fe_3O_4 and metallic TiN. Nikolaev and co-workers[6] have measured the MR and magnetic coupling (MC) in superlattices of $La_{2/3}Ba_{1/3}MnO_3$ and $LaNiO_3$ (LNO). The hole-doped manganite LBMO is ferromagnetic with a metal-like conductivity below $T_c \sim 340$ K,[13] and the nicolate LNO is a metallic paramagnet down to 4.2 K.[14] In superlattices consisting of a fixed LBMO layer thickness (12 UC), Nikolaev *et al.*[6] observe oscillatory exchange coupling as the LNO thickness is varied from 3 to 10 unit cells. While these authors also observe a positive magnetoresistance in antiferromagnetically coupled superlattices at 5 K, oscillations in MR commensurate with the MC (Ref. 2) are not seen. Venimadhav *et al.*[15] also reported electrical and magnetic properties of the superlattices consisting of a ferromagnetic manganite ($La_{0.6}Pb_{0.4}MnO_3$) and a metallic but nonsuperconducting cuprate $La_4BaCu_5O_{13+x}$. They observed monotonic behavior of the Curie temperature and saturation field in these multilayers as the cuprate layer thickness is increased from 1 to 8 unit cells, while keeping the thickness of the manganite fixed at 10 UC. Interestingly, these samples exhibit semiconductorlike resistivity ($d\rho/dT$ negative) down to 4.2 K, although thin films of individual oxides are metallic below 300 K. However, to our best knowledge, similar measurements of resistivity over a broad temperature range in systems where oscillatory coupling is observed are not available. It is certainly of interest to know if the resistivity of such systems is also insulating at low temperatures. The semiconductorlike behavior observed by Venimadhav *et al.*[15] suggests disordered interfaces in these thin-film multilayers. A sufficiently disordered interface can suppress the metal-like transport in individual constituents. This disorder can be of magnetic as well as structural origin. The magnetic and structural inhomogeneities at the interfaces can dominate the contribution of fundamental processes such as the Ruderman-Kittel-Kasuya-Yosida interaction and spin-polarized tunneling to magnetic coupling[3] and transport in these artificial structures.

In this paper we examine the temperature dependence of the electrical resistivity of the ferromagnetic manganite $La_{0.7}Ca_{0.3}MnO_3$ based superlattice as the thickness of the $LaNiO_3$ spacer layer is varied. We first measured the $\rho(T)$ curves for individual films of LCMO and LNO with thicknesses ranging from small $\sim$10 to $\sim$100 UC. Here the thickness is written in units of the pseudocubic lattice parameters of 3.86 and 3.83 Å for LCMO and LNO, respectively. The resistivity of both the materials at small thicknesses shows the contribution of thin-film size effects such as a large room-temperature value and insulatorlike behavior at low temperatures. In the $\{[(\text{LCMO})\ 10\text{-unit-cell}]/[(\text{LNO})\ n\text{-unit-cell}]\}\times 15$ superlattices, where the cumulative thickness of LCMO and LNO is large enough to see a bulklike transport, a semiconductorlike resistivity is seen for $n \leqslant 4$. The superlattices with $n \leqslant 4$ also show a large negative magnetoresistance at low temperatures. Samples with $n > 5$ are metallic over the entire range of temperatures. A discussion of these features is presented in light of struc-

tural data and the effects of interfacial strain. Our analysis strongly suggests that the magnetic and structural disorders at the interfaces of LCMO and LNO lead to a transition from insulator-to-metallike behavior with increasing n, and the large low-temperature magnetoresistance is seen in the sample with $n<5$. A simple parallel resistor model, where we explicitly incorporate the resistivity of the disordered regions, reproduces the broad features of the $\rho(T)$ curves.

II. EXPERIMENT

We have used a multitarget pulsed laser deposition (PLD) system for the growth of LCMO and LNO thin films and LCMO/LNO superlattices on (001) $SrTiO_3$ (STO) and (001) $LaAlO_3$ (LAO) substrates. The bulk targets of stoichiometric composition of LCMO and LNO were prepared by the solid-state reaction method.[16,17] The individual thin films of LCMO and LNO, and the multilayers, were deposited at 750 °C in an oxygen ambient of 400 mTorr. The deposition rates (typically ~2.0 Å/sec) of LCMO and LNO were calibrated for each laser pulse of energy density ~3 J/cm^2. After completion of deposition, the chamber was backfilled to atmospheric pressures and the sample was cooled to room temperature at the rate of ~5 °C/min. For studies of electron transport in individual films, samples of LCMO of different thicknesses were deposited directly onto (001) LAO and STO. In the case of LNO, however, a buffer layer of 20 unit-cell-thick LCMO was used. The superlattice structures were synthesized by repeating 15 times the bilayer comprising of 10-(UC) LCMO and n-(UC) LNO, with n taking integral values from 2 to 10. The first layer to be deposited on the substrate was 10-(UC) LCMO. The analytical techniques used to characterize the chemical composition of the films include x-ray diffraction, Rutherford backscattering, and electron probe microanalysis.[17,18] The epitaxial growth, and the presence of superstructures in the multilayers and the single-layer epitaxy of their constituents, were confirmed by x-ray diffraction using a θ-ω diffractometer operated in θ-2θ mode. Measurements of electrical resistivity in the range 4.2–350 K were carried out in a variable-temperature cryostat equipped with a 4-T superconducting solenoid. A four-probe method, with sufficiently large distance between the voltage and current tabs, was used for resistivity measurements. Contacts were made by evaporating silver over the edges of the current and voltage tabs to ensure uniform flow of current through all units of the multilayers. The measurements of magnetoresistance were carried out with magnetic field applied parallel to the direction of the current in the sample.

III. RESULTS

In Fig. 1 we show the diffracted x-ray intensity from two superlattices with LNO layer thickness of 4 and 8 unit cells deposited on LAO [curves (a) and (b)] and STO [curves (c) and (d)] substrates, respectively. The 2θ range scanned here includes the (001) reflection of these pseudocubic perovskites. The presence of two satellite peaks on either side of the fundamental (001) diffraction clearly show a periodically

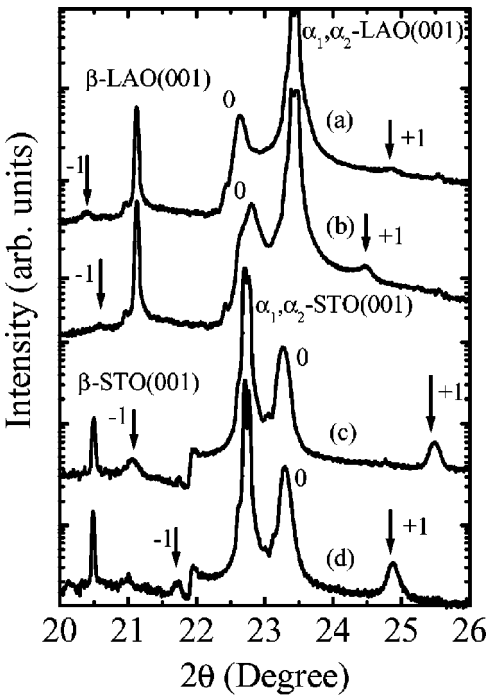

FIG. 1. Copper K_α–x-ray-diffraction profiles of $[(10\text{-UC})\ \text{LCMO}/(n\text{-UC})\ \text{LNO}]_{15}$ superlattices with $n=4$ and 8 grown on (001)-oriented $LaAlO_3$ [curves (a) and (b)] and on (001)-oriented $SrTiO_3$ [curves (c) and (d)]. The fundamental (001) reflection of the film is marked as "0." The first-order satellites on either side of this reflection are marked as $+1$ and -1. The figure also shows (001) reflection of the substrate due to K_α and K_β excitation.

modulated structure.[19,20] The intensity of the satellite peaks is stronger in the case of the superlattices deposited on the STO substrates. The intensity of higher-order satellites is not significant, presumably due to a small electron-density difference in LCMO and LNO. The lattice parameters [curve (a), Fig. 1] of LCMO and LNO in the bulk are 3.86 and 3.83 Å, respectively, whereas for the substrates we have $a_{\text{LAO}}=3.79$ and $a_{\text{STO}}=3.90$ Å. Clearly, the in-plane lattice parameter of the superlattices is under expansion on LAO and is in compression on STO. Our data on all superlattices ($n=2-10$) show that the c-axis lattice parameter approaches the bulk value as the thickness increases with n. We also notice a distinct broadening of the (001) peak as the relative fraction of the LNO and LCMO unit cells becomes unity.

Before we discuss the resistivity of the multilayers, it is worthwhile to investigate electrical conduction in the constituent films. In Fig. 2(a) we show the $\rho(T)$ data for six LCMO films of different thicknesses (32 to 100 UC) deposited on LAO. The zero-field resistivity of the four thicker films shows the characteristic thermally activated behavior in the high-temperature paramagnetic state followed by an insulator-metal transition at the Curie temperature (T_c). The room-temperature resistivity of the films increases and the T_c drops as their thickness is reduced. At very small thicknesses, (~50 UC), the thermally activated behavior continues down to the lowest temperature with no indication of a peak near T_c. This critical thickness, below which no metallike resistivity is seen, is smaller for the films deposited on

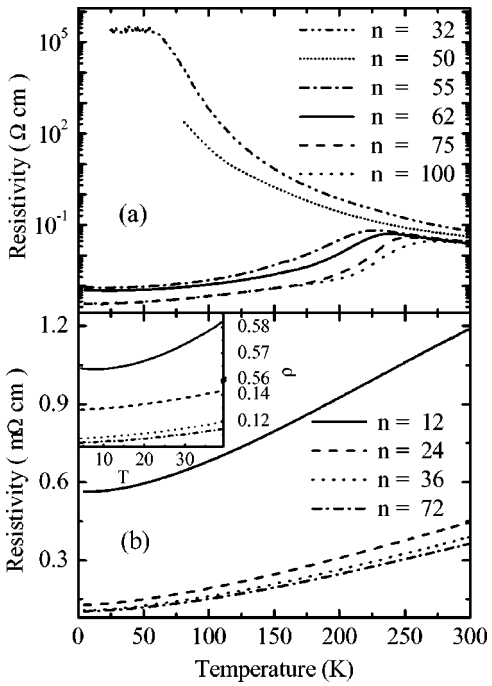

FIG. 2. (a) Zero-field electrical resistivity of LCMO films of different thicknesses deposited on (001)-oriented LAO. Film thickness is written in units of the pseudocubic lattice parameter $a = 3.86$ Å. Zero-field electrical resistivity of $LaNiO_3$ films is shown in (b). Here $n = 1$ corresponds to 3.83 Å. Inset of (b) shows the resistivity of LNO films in the temperature range 4.2–40 K.

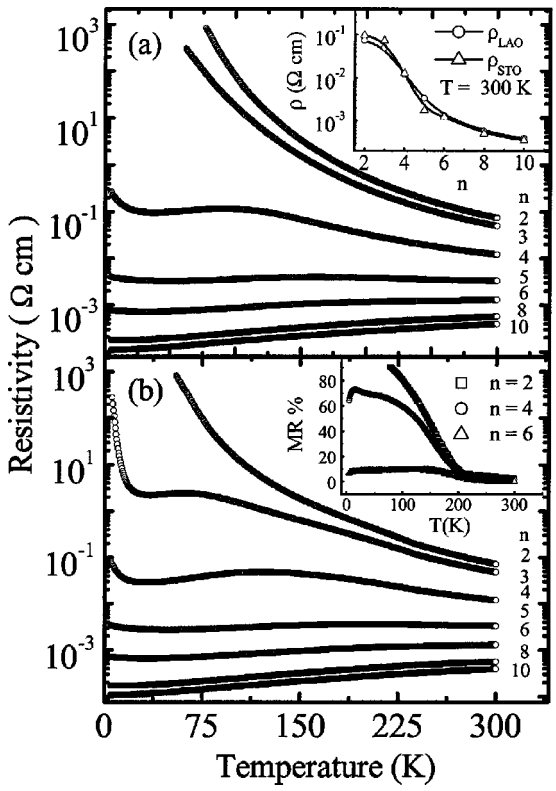

FIG. 3. (a) Zero-field in-plane electrical resistivity of $[(10\text{-UC})\ LCMO/(n\text{-UC})\ LNO]_{15}$ superlattices grown on (001)-oriented LAO with different spacer layer thicknesses. Inset shows variation of room-temperature resistivity of the superlattices deposited on STO and LAO as a function of LNO spacer layer thickness. (b) In-plane electrical resistivity of same superlattices in 4-T magnetic field applied in the plane of the film. Inset shows the variation of MR $\{(\Delta\rho/\rho)\times 100 = [(\rho - \rho_H)/\rho]\times 100\}$ with temperatures for superlattices with $n = 2$, 4, and 6.

STO.[18] The thicker (>50 UC) LCMO films measured here show a large negative magnetoresistance in the vicinity of the Curie temperature.

The bulk LNO is a metallic paramagnet down to helium temperatures.[14] In Fig. 2(b) we show the electrical resistivity of four LNO films of thicknesses 12, 24, 36, and 72 unit cells deposited on LAO with a 20-UC buffer layer of LCMO. The room-temperature resistivity of LNO films is smaller by a factor of ~65 as compared to the resistivity of the LCMO film of the same thickness. The resistivity of LNO films shows characteristic size effects on lowering thickness. However, $\rho(T)$ remains metallic down to 4.2 K for films $n > 24$ as evident in the inset of Fig. 2. In the case of the thinnest film ($n = 12$), we observe an upturn in the resistivity curve at the lowest temperature. In the presence of a 4-T field collinear with the current, these films show a negligible magnetoresistance.

Having investigated the behavior of $\rho(T)$ in thin films of LCMO and LNO, we now present results of our measurements on the superlattices. Figure 3(a) shows the zero-field $\rho(T)$ curves for seven samples with different spacer layer thickness. For the samples with $n = 2$ and 3, the resistivity is thermally activated down to ~100 K. Below this temperature, the resistivity of the films becomes so large that a constant current technique of measurement does not work due to impedance limitations of our voltmeter. While a similar behavior has been observed in metallic manganite-based superlattices, the spacer material in these cases was an insulator.[8–12] On increasing the LNO layer thickness to 4 unit cells, the $\rho(T)$ is first thermally activated down to ~100 K and then becomes metal-like (positive $d\rho/dT$) in the temperature window of 25–100 K. At $T < 25$ K, $\rho(T)$ is again thermally activated. A qualitatively similar behavior, albeit with a wider metal-like window, is seen for the sample with $n = 5$. The $\rho(T)$ curves remain metallic over the entire temperature range for the sample with $n \geq 6$. Clearly, an insulator-to-metal transition is seen in these superlattices in the vicinity of $n = 5$. We have also measured the resistivity of the multilayers deposited on STO simultaneously with the samples on LAO. The qualitative features of the $\rho(T)$ data for these samples are similar to those shown in Fig. 3(a). In the inset of Fig. 3(a) we show the variation of room-temperature resistivity of the multilayers as a function of spacer layer thickness. The resistivity of the films on STO is higher by a small fraction.

Figure 3(b) shows the resistivity of the superlattices measured in a 4-T field. The in-field resistivity of the sample with $n = 2$ drops significantly from its zero-field value [Fig. 3(a)]. However, its temperature dependence remains thermally activated down to 4.2 K. The resistivity of the samples with $n = 3$ undergoes a remarkable change on application of the field. In addition to a large negative magnetoresistance,

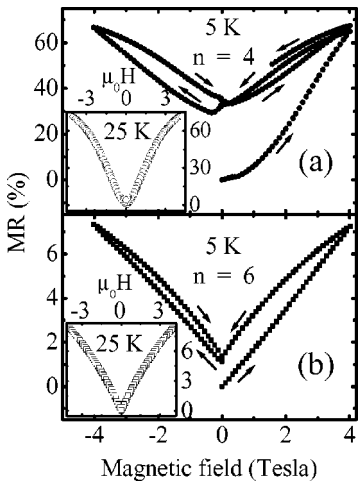

FIG. 4. (a) Magnetic-field dependence of MR in $n=4$ superlattice at 5 K. The sample was first zero-field cooled to 5 K and then the magnetic field was scanned from zero to +4 T followed by cyclic sweeps between +4 and −4 T. Inset shows field dependence of MR at 25 K. (b) 5-K MR of the $n=6$ superlattice. Field sweep directions are shown by arrows. Inset shows MR at 25 K.

the $\rho(T)$ curve is also metal-like ($d\rho/dT$ positive) over a narrow range of temperatures (25–65 K). The drop in resistivity at ~65 K suggests onset of magnetic ordering in the LCMO layers of the superlattice. For the sample with $n=4$, the window of temperature over which a metal-like resistivity is seen widens on application of the field. In the case of the samples with $n>5$, no appreciable change in the resistivity is seen on application of the field. In the inset of Fig. 3(b), we plot the magnetoresistance $[(\rho\text{-}\rho_H)/\rho\times 100$, where ρ_H and ρ are in-field and zero-field resistivities of the samples] with $n=2$, 4, and 6. The MR of the superlattices with $n\leqslant 6$ shows a rapid increase upon lowering temperature below ~200 K. While the MR of the $n=2$ sample could not be measured below ~100 K, in samples with $n=3$ and 4 it first saturates and then drops below ~20 K. This is unlike the case of a typical ferromagnetic manganite where the MR is maximum near T_c.[21] Also the MR is significantly higher in the superlattices.

In Figs. 4(a) and 4(b) we show the behavior of zero-field-cooled (ZFC) MR in $n=4$ and 6 multilayers as the magnetic field is swept over a complete cycle between +4 and −4 T. As seen in the insets, the MR of both samples at 25 K first increases rapidly and then tends to saturate at the highest field. Absence of a hysteresis in these data suggests free rotation of magnetization vectors in each LCMO layer. However, the field dependence of MR at temperatures below ~20 K shows strong hysteretic effects [5-K data are shown in Figs. 4(a) and 4(b)]. These low-temperature hysteretic effects in ZFC magnetoresistance suggest pinning of LCMO magnetization by the disordered interfacial phase. In the sample with $n=4$, we also notice that the MR during the second field sweep from +4 T to zero field does not trace the path taken during the first sweep. This indicates a weak magnetorelaxor-type behavior seen earlier in $La_{0.5}Ca_{0.5}Mn_{1-x}Cr_xO_3$ films.[22]

IV. DISCUSSION

The large room-temperature resistivity and its thermally activated nature in superlattices with $n<4$ is puzzling. The cumulative thickness of LCMO in these samples is well above the threshold for metallic behavior in LCMO films.[18] A comparison with the data for individual films (Fig. 2) suggests that $\rho(T)$ of these superlattices should, in fact, have a well-defined peak near the Curie temperature (T_c) and a metal-like behavior below T_c. However, this scenario is applicable only under the assumption that the multilayers have a coherent *c*-axis growth with no interfacial disorder. Two possible mechanisms for the interfacial disorder can be identified. One is of a metallurgical origin where intermixing of the constituent elements of LCMO and LNO takes place at the interface. The ensuing randomization of the magnetic ions (Mn and Ni) at the interface would also result in magnetic disorder. The extent of interfacial mixing can be evaluated through analysis of x-ray-diffraction data[23,24] and by making use of high-resolution cross-sectional electron microscopy.[24,25] The interfaces of multicomponent oxide-based superlattices such as those of high-T_c cuprates and manganites prepared using magnetron sputtering, PLD, and molecular-beam epitaxy (MBE) have been studied using these techniques.[23–26] Further, the layer-by-layer growth of multilayers has also been studied *in situ* with high- or low-energy electron diffraction in PLD (Ref. 26) and MBE (Ref. 6) processes. These studies suggest that the interfaces of oxide multilayers are relatively sharp. While we have not undertaken a detailed study of interfacial mixing, we expect it to be negligible since our deposition conditions are similar to those used in studies where the interfaces have been analyzed in detail.[25,26] However, even if the interfaces are ideally terminated, they will always have magnetic disorder. This is because of the changes in the nearest-neighbor environment of the magnetic ions at interfaces and modification of bond angles and bond distances caused by the interfacial strain. There are two important consequences of the magnetic disorder. First, we see a local breakdown of the double exchange mechanism,[27] which is responsible for metallic conduction in LCMO below T_c, and secondly, the disorder can also affect the metallic character of $LaNiO_3$. Noticeably, this cubic perovskite tends to have a charge ordered insulation ground state as the La sites are replaced by ions of smaller radii such as Nd^{3+}, Sm^{3+}, etc.[28] While the thickness of this magnetically and electrically altered interfacial region will decrease as the lattice mismatch is reduced, it is likely to remain nonzero due to magnetic ions even when the lattice parameters of the constituents are identical. Our earlier work on ultrathin films of LCMO (Ref. 18) indicates that the disorder region at the film-substrate interface is wider in the case of LAO (mismatch$\sim+1.8\%$) than in LCMO films on STO (mismatch$\sim-1.0\%$). In the case of the multilayers, however, the width of the disordered region is decided by the mismatch between LCMO and LNO ($\delta a/a\sim+0.8\%$). This is perhaps the reason why properties of the multilayers on STO and LAO are remarkable similar.

We have successfully modeled the resistivity of the superlattices by explicitly taking into account the contribution of

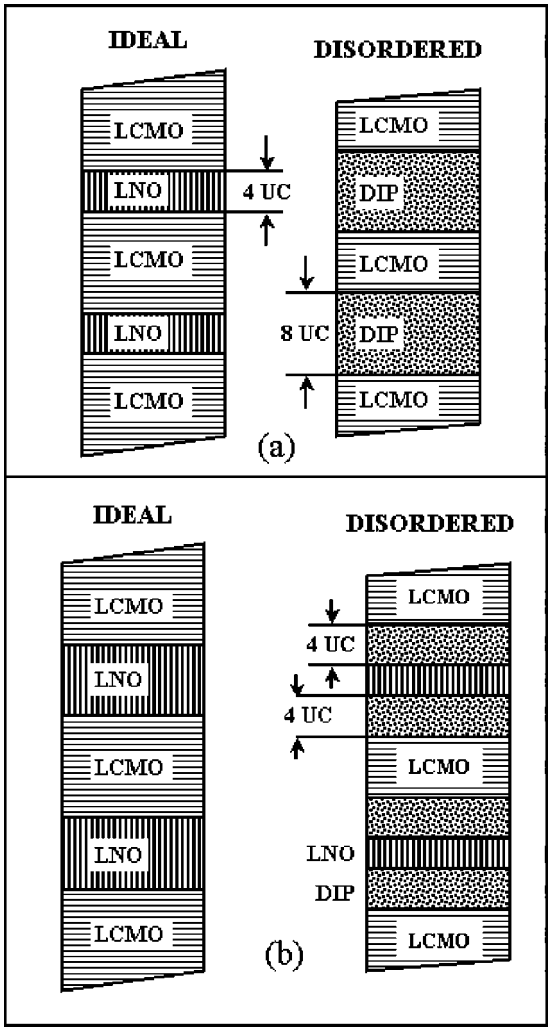

FIG. 5. (a) A schematic view of the cross section of the multilayer with $n=4$. Left-hand side of the figure shows atomically sharp interfaces. Cross section of the same multilayer with interfacial disorder is shown on the right. (b) shows the cross section of multilayers with $n>4$ is in the clean (left-side) and disordered (right-side) limits. The disorder is assumed to consume 2 unit cells of the film on both sides of the interface.

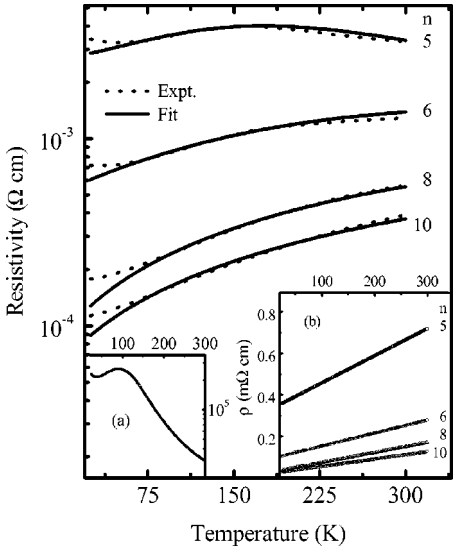

FIG. 6. The measured and calculated resistivities of the superlattices with $n=5$, 6, 8, and 10. The calculation is based on a parallel resistor model for a stack of 15 quad layers, each consisting of LCMO, LNO, and the disordered interfacial phase. The resistivity of the interfacial phases deduced from $\rho(T)$ data of the superlattice with $n=4$ is plotted in the inset (a). (b) shows the resistivity of LNO layers $[\rho(T)=\rho_0+\rho_1 T]$ obtained from the best fits (see text for detail).

the interfacial region to total conduction. We first assume that 2-UC-thick samples of LCMO and LNO on either side of the interface convert to the disordered phase. The superlattice with $n=4$ then consists of a stack of 15 bilayers of LCMO and the disordered interfacial phase (DIP) as sketched in Fig. 5(a). From the measured resistivity of the superlattice with $n=4$ and the resistivity of the 32-UC-thick LCMO film at various temperatures, we extract, using a parallel resistor model, the temperature dependence of the resistivity of the DIP. The result of this calculation is shown in the inset of Fig. 6. Here it is important to point out that the resistivity of the disordered phase has an unphysical sign (negative) if the $\rho(T)$ of LCMO layers is taken to be that of a thicker film [one with a well-defined Curie temperature and positive $d\rho/dT$ at $T<T_c$ as shown in Fig. 2(a)]. Under this model, the superlattices with $n>4$ consist of 15 identical quad layer units as shown in Fig. 5(b). Here, while the thicknesses of LCMO and the DIP remain the same, the LNO thickness increases with n. In these periodic quad layer structures it is also reasonable to argue that the resistivities of LCMO and the DIP do not change with n. However, this is certainly not true for the LNO as the LNO layer thickness increases with n. The data of Fig. 2(a) suggest that the resistivity of LNO should decrease as n increases. In Fig. 6 we show the measured and calculated resistivity of the samples with $n=4$, 6, 8, and 10. Here we have taken the resistivity of LNO as $\rho_{\mathrm{LNO}}(T)=\rho_0+\rho_1 T$, with ρ_0 and ρ_1 as temperature-independent adjustable parameters. The resistivity of the DIP and LCMO are the same as used in the calculations for multilayers with $n=4$. As evident in the figure, the measured and calculated resistivities are in excellent agreement above $\sim$75 K. The disagreement at $T<75$ K is perhaps due to the fact that our calculation does not take into account the upturn in the resistivity of thin LNO films at lower temperatures. In the inset of Fig. 6 we show the calculated $\rho_{\mathrm{LNO}}(T)$ for different superlattices. The similarity of these curves with the data on individual films of LNO [Fig. 2(b)] is noteworthy.

The large negative magnetoresistance at lower temperatures in samples with $n\leqslant 4$ highlights the sensitivity of electron transport in the disordered interfacial phase to a magnetic field. While this effect should be present in samples of larger n as well, observing it may be difficult because of the shunting of current paths by the much more conducting LNO layers. The DIP on the LCMO side may consist of pinned t_{2g} spins of the Mn^{3+} and Mn^{4+} ions, which may tend to bias the magnetization of the LCMO layer. Randomly oriented magnetic moments of LCMO layers are likely to inhibit transport of spin-polarized carriers across LCMO-LNO interfaces.[29,30] At lower temperatures, the depinning of these

ionic spins and concomitant parallel alignment of LCMO moments may require substantial fields. However, higher temperatures tend to marginalize the pinning. This is perhaps why the MR decreases at higher temperatures. The interfacial disorder can also lead to distortion of NiO_6 octahedra in the $LaNiO_3$ layers. It is well known that deviations from a perfect cubic symmetry can open up a charge order gap in this rare-earth nicolate.[28] Electrical conduction in the resulting antiferromagnetic and insulating state would show a considerable sensitivity to magnetic field.

V. CONCLUSION

In conclusion, we have measured the electrical resistivity and magnetoresistance of LCMO/LNO multilayers with different LNO layer thicknesses over a 4.2–300 K temperature range. Multilayers with LNO thickness <5 unit cells show a thermally activated resistivity over the entire temperature range. These samples also show a large magnetoresistance, which grows with decreasing temperature. A parallel resistor model, where in the resistance of the disordered interfacial region is considered explicitly, reproduces the broad features of the $\rho(T)$ curves. We attribute the disordered interfacial region to lattice-mismatch-related strain and truncation of the 3D coordination of magnetic ions at the LCMO-LNO interfaces. A field-assisted transport of spin-polarized carriers across the interfaces and hopping of e_g electrons between Mn^{3+} and Mn^{4+} ions, whose t_{2g} spins are pinned by the interfacial disorder, provides a plausible scenario for the large low-temperature magnetoresistance.

ACKNOWLEDGMENT

This research has been supported by a grant from the Science and Engineering Research Council of the Department of Science and Technology, Government of India.

[1] M. N. Baibich, J. M. Broto, A. Fert, F. Nguyen Van Dau, F. Petroff, P. Eitenne, G. Creuzet, A. Friederich, and J. Chazelas, Phys. Rev. Lett. **61**, 2472 (1988).
[2] S. S. P. Parkin, N. More, and K. P. Roche, Phys. Rev. Lett. **64**, 2304 (1990).
[3] *Ultrathin Magnetic Structures II*, edited by B. Heinrich and J. A. C. Bland (Springer-Verlag, Berlin, 1994).
[4] G. Q. Gong, A. Gupta, Gang Xiao, P. Lecoeur, and T. R. McGuire, Phys. Rev. B **54**, 3742 (1996).
[5] A. Orozco, S. B. Ogale, Y. H. Li, P. Fournier, Eric Li, H. Asano, V. Smolyaninova, R. L. Greene, R. P. Sharma, R. Ramesh, and T. Venkatesan, Phys. Rev. Lett. **83**, 1680 (1999).
[6] K. R. Nikolaev, A. Yu. Dobin, I. N. Krivorotov, W. K. Cooly, A. Bhattacharya, A. L. Kobrinskii, L. I. Glazman, R. M. Wentzovitch, E. Dan Dahlberg, and A. M. Goldman, Phys. Rev. Lett. **85**, 3728 (2000); K. R. Nikolaev, A. Bhattacharya, P. A. Kraus, V. A. Vas'ko, W. K. Cooley, and A. M. Goldman, Appl. Phys. Lett. **75**, 118 (1999).
[7] G. Jakob, V. V. Moshchalkov, and Y. Bruynseraede, Appl. Phys. Lett. **66**, 2564 (1995).
[8] I. Panagiotopoulos, C. Christides, M. Pissas, and D. Niarchos, Phys. Rev. B **60**, 485 (1999).
[9] Moon-Ho Jo, Neil D. Mathur, Jan E. Evetts, Mark G. Blamire, Manuel Bibes, and Josep Fontcuberta, Appl. Phys. Lett. **75**, 3689 (1999).
[10] M. Izumi, Y. Murakami, Y. Konishi, T. Manako, M. Kawasaki, and Y. Tokura, Phys. Rev. B **60**, 1211 (1999).
[11] C. Kwon, K.-C. Kim, M. C. Robson, J. Y. Gu, M. Rajeswari, T. Venkatesan, and R. Ramesh, J. Appl. Phys. **81**, 4950 (1997).
[12] H. Li, J. R. Sun, and H. K. Wong, Appl. Phys. Lett. **80**, 628 (2002).
[13] R. von Helmolt, J. Wecker, B. Holzapfel, L. Schultz, and K. Samwer, Phys. Rev. Lett. **71**, 2331 (1993).
[14] J. B. Goodenough, N. F. Mott, M. Pouchard, G. Demazeau, and P. Hagenmüller, Mater. Res. Bull. **8**, 647 (1973).
[15] A. Venimadhav, M. S. Hegde, R. Rawat, I. Das, P. L. Paulose, and E. V. Sampathkumaran, Phys. Rev. B **63**, 214404 (2001).
[16] Chaitali Roy and R. C. Budhani, J. Appl. Phys. **85**, 3124 (1999).
[17] R. C. Budhani, N. K. Pandey, P. Padhan, S. Srivastava, and R. P. S. M. Lobo, Phys. Rev. B **65**, 014429 (2002).
[18] P. Padhan, N. K. Pandey, S. Srivastava, R. K. Rakshit, V. N. Kulkarni, and R. C. Budhani, Solid State Commun. **117**, 27 (2001).
[19] Ivan K. Schuller, Phys. Rev. Lett. **44**, 1597 (1980).
[20] B. Y. Jin and J. B. Ketterson, Adv. Phys. **38**, 189 (1989).
[21] Myron B. Salamon and Marcelo Jaime, Rev. Mod. Phys. **73**, 583 (2001).
[22] Y. Ogimoto, M. Izumi, T. Manako, T. Kimura, Y. Tomioka, M. Kawasaki, and Y. Tokura, Appl. Phys. Lett. **78**, 3505 (2001).
[23] Eric E. Fullerton, Ivan K. Schuller, H. Vanderstraeten, and Y. Bruynseraede, Phys. Rev. B **45**, 9292 (1992).
[24] J.-M. Triscone and Ø. Fischer, Rep. Prog. Phys. **60**, 1673 (1997).
[25] C. B. Eom, A. F. Marshall, J.-M. Triscone, B. Wilkens, S. S. Laderman, and T. H. Geballe, Science **251**, 780 (1991).
[26] M. Izumi, T. Manako, Y. Konishi, M. Kawasaki, and Y. Tokura, Phys. Rev. B **61**, 12 187 (2000); M. Izumi, Y. Konishi, T. Nishihara, S. Hayashi, M. Shinohara, M. Kawasaki, and Y. Tokura, Appl. Phys. Lett. **73**, 2497 (1998).
[27] C. Zener, Phys. Rev. **81**, 440 (1951).
[28] J. B. Torrance, P. Lacorre, A. I. Nazzal, E. J. Ansaldo, and Ch. Niedermayer, Phys. Rev. B **45**, 8209 (1992).
[29] Mark Johnson, Phys. Rev. Lett. **67**, 3594 (1991).
[30] T. Valet and A. Fert, Phys. Rev. B **48**, 7099 (1993).